別紙４

研究成果の刊行に関する一覧表

雑誌

発表者氏名	論文タイトル名	発表誌名	巻号	ページ	出版年
Ichikawa H, Yoshida A, Kanda T, Kosugi SI, Ishikawa T, Hanyu T, Taguchi T, Sakumoto M, Katai H, Kawai A, Wakai T, Kondo T	Prognostic significance of promyelocytic leukemia expression in gastrointestinal stromal tumor; integrated proteomic and transcriptomic analysis.	Cancer Sci.	doi: 10.1111/cas.12565.		2014
Taoka M, Morofuji N, Yamauchi Y, Ojima H, Kubota D, Terukina G, Nobe Y, Nakayama H, Takahashi N, Kosuge T, Isobe T, Kondo T	Global PROTOMAP Profiling to Search for Biomarkers of Early-Recurrent Hepatocellular Carcinoma.	J Proteome Res.	7;13(11):	4847-58.	2014
Hosoya N, Sakumoto M, Tomita Y, Kondo T	Approach to spot overlapping problem in 2D-PAGE revealed clinical and functional signature of RKIP and MnSOD in renal cell.	EuPA Open Proteomics.	4	129-139.	2014
Kubota D, Yoshida A, Kawai A, Kondo T	Proteomics identified overexpression of SET oncogene product and possible therapeutic utility of protein phosphatase 2A in alveolar soft part sarcoma.	J Proteome Res.	2;13(5):	2250-61.	2014
Mimae T, Ito A, Hagiyama M, Nakanishi J, Hosokawa Y, Okada M, Murakami Y, Kondo T	A novel approach to pseudopodia proteomics: excimer laser etching, two-dimensional difference gel electrophoresis, and confocal imaging.	Protoc exch.	4;2014.	pii:2014.007.	2014
Ichikawa H, Kanda T, Kosugi S, Kawachi Y, Wakai T, Kondo T	Proteomic and meta-transcriptomic study on lymph node metastasis in gastric cancer.	EuPA Open Proteomics.	3	183-94.	2014
Mizutani, T., Ishizaka, A., Suzuki, Y., and Iba, H	7SK small nuclear ribonucleoprotein complex is recruited to the HIV-1 promoter via short viral transcripts.	FEBS Letters	588	1630-1636	2014

Kobayashi, K.,Sakurai, K., Hiramatsu, H.,Inada, K., Shiogama, K.,Nakamura, S., Suemasa, F., Kobayashi, K.,Imoto, S., Haraguchi, T., Ito, H., Ishizaka, A., Tsutsumi, Y., & Iba H	The miR-199a/Brm/EGR1 axis is a determinant of anchorage-independent growth in epithelial tumor cell lines.	Scientific Reports		In press	2015
Fujiwara T,Katsuda T, Hagiwara K, Kosaka N, Yoshioka Y, Takahashi RU, Takeshita F, Kubota D, Kondo T, Ichikawa H, Yoshida A, Kobayashi E, Kawai A, Ozaki T, Ochiya T	Clinical relevance and therapeutic significance of microRNA-133a expression profiles and functions in malignant	osteosarcoma-initiating cells. Stem Cells	32	959–973	2014
Fujiwara T, Kawai A, Nezu Y, Fujita Y, Kosaka N, Ozaki T,Ochiya T	Circulating microRNAs in sarcoma: potential biomarkers for diagnosis and targets for therapy.	Chemotherapy	3:1000123		2014
Fujiwara T, Kunisada T, Takeda K, Uotani K, Yoshida A, Ochiya T, Ozaki T	MicroRNAs in soft tissue sarcomas: overview of the accumulating evidence and importance as novel biomarkers.	Biomed Res Int	2014:592868	1-15	2014
Fujiwara T, Takahashi RU, Kosaka N, Nezu Y, Kawai A, Ozaki T, Ochiya T	RPN2 gene confers osteosarcoma cell malignant phenotypes and determines clinical prognosis.	Mol Ther Nucleic Acids	3:e189		2014
Osaki M, Kosaka N, Okada F, Ochiya T	Circulating microRNAs in drug safety assessment for hepatic and cardiovascular toxicity: the latest biomarker frontier?	Mol Diagn The	18	121-126	2014

Ⅳ. 研究成果の刊行物

Cancer Science
Japanese Cancer Association JCA
Open Access

Prognostic significance of promyelocytic leukemia expression in gastrointestinal stromal tumor; integrated proteomic and transcriptomic analysis

Hiroshi Ichikawa,[1,2] Akihiko Yoshida,[3] Tatsuo Kanda,[4] Shin-ichi Kosugi,[2] Takashi Ishikawa,[2] Takaaki Hanyu,[2] Takahiro Taguchi,[5] Marimu Sakumoto,[1] Hitoshi Katai,[6] Akira Kawai,[7] Toshifumi Wakai[2] and Tadashi Kondo[1]

[1]Division of Pharmacoproteomics, National Cancer Center Research Institute, Tokyo; [2]Division of Digestive and General Surgery, Niigata University Graduate School of Medical and Dental Sciences, Niigata; [3]Department of Pathology and Clinical Laboratories, National Cancer Center Hospital, Tokyo; [4]Department of Surgery, Sanjo General Hospital, Niigata; [5]Research and Education Faculty, Multidisciplinary Science Cluster, Kuroshio Science Unit, Kochi; [6]Division of Surgical Oncology, National Cancer Center Hospital, Tokyo; [7]Division of Musculoskeletal Oncology, National Cancer Center Hospital, Tokyo, Japan

Key words

Gastrointestinal stromal tumor, promyelocytic leukemia, proteomics, transcriptomics, tumor site

Correspondence

Tadashi Kondo, Division of Pharmacoproteomics, National Cancer Center Research Institute, 5-1-1 Tsukiji, Chuo-ku, Tokyo 104-0045, Japan.
Tel: +81-3-3542-2511 ext. 3004; Fax: +81-3547-5298;
E-mail: takondo@ncc.go.jp

Funding Information

This work was supported by the National Cancer Center Research Core Facility and the National Cancer Center Research and Development Fund (23-A-7 and 23-A-10).

Received August 15, 2014; Revised October 15, 2014; Accepted October 18, 2014

Cancer Sci **106** (2015) 115–124

doi: 10.1111/cas.12565

Prognostic markers are urgently needed to optimize the postoperative treatment strategies for gastrointestinal stromal tumors (GIST). GIST of the small intestine (I-GIST) show more aggressive behavior than those of the stomach (S-GIST), and the molecular background of the malignancy in I-GIST may include potential prognostic biomarkers. We conducted integrated proteomic and transcriptomic analysis to identify genes showing differential expressions according to the tumor site. We generated protein expression profiles for four cases each of surgically resected I-GIST and S-GIST using label-free proteomic analysis. For proteins showing differential expressions, global mRNA expression was compared between 9 I-GIST and 23 S-GIST. Among the 2555 genes analyzed, we found that promyelocytic leukemia (*PML*), a tumor suppressor gene, was significantly downregulated in I-GIST at both the protein and mRNA levels ($P < 0.01$; fold difference ≥2.0). Immunohistochemistry of 254 additional cases from multiple clinical facilities showed that PML-negative cases were significantly frequent in the I-GIST group ($P < 0.001$). The 5-year recurrence-free survival rate was significantly lower in the PML-negative than in the PML-positive cases (60.1% *vs* 91.7%; $P < 0.001$). Multivariate analysis revealed that downregulation of PML was an independent unfavorable prognostic factor (hazard ratio = 2.739; $P = 0.001$). Our study indicated that prognostication based on PML expression may have potential for optimizing the treatment strategy for GIST patients. Further validation studies of PML for clinical application, and investigation for the mechanistic significance of PML to clarify the molecular backgrounds of malignancy in GIST are warranted.

Gastrointestinal stromal tumors (GIST) are a common type of soft-tissue sarcoma.[1] Approximately 75–80% of GIST harbor an activating mutation in the *KIT* oncogene and 5–8% in platelet-derived growth factor receptor-α (*PDGFRA*), which are both key molecular drivers of GIST pathogenesis.[2–5] Adjuvant therapy with imatinib, a tyrosine kinase inhibitor, prolongs recurrence-free survival (RFS) after complete resection.[6,7] Recently, a randomized trial revealed that patients with a high-risk of recurrence show longer survival with 3 years of imatinib administration than with 1 year.[8] Almost all patients receiving imatinib therapy suffer some adverse effects, and approximately 50% of the operative GIST patients are cured by surgery alone.[8] Therefore, prognostic markers are needed to optimize adjuvant imatinib therapy.[9]

Gastrointestinal stromal tumor arise predominantly in the stomach (60–70%) and small intestine (20–30%).[10] GIST of the small intestine (I-GIST) show more aggressive behavior than those of the stomach (S-GIST), with similar size and mitotic activity.[11] Therefore, the tumor site is included as a factor in currently employed risk stratification schemes.[12] Investigations of genetic aberrations that are specific to tumors arising at certain anatomical sites can provide clues to understanding the molecular mechanisms of malignant behavior of GIST, thus leading to the development of prognostic biomarkers. It has been reported that differences in expression or mutation of *KIT* and *PDGFRA* are associated with the tumor site.[13,14] In addition, chromosomal aberrations and gene expressions that are specific to I-GIST have been identified in genome-wide global studies, and these have also been shown to be adverse prognostic factors.[15–20] However, these reports lack validation studies for the confirmation of the prognostic value and clinical utility. Therefore, intensive validation studies, including multi-institutional research, are needed to establish the prognostic biomarkers from tumor site-specific genes.

In the present study, we aimed to identify the molecular backgrounds specific to the tumor site and to discover the prognostic biomarker in GIST. We integrated proteomic and transcriptomic analysis, and observed a total of 2555 genes. For the proteomic analysis, we applied a label-free proteomics, allowing comprehensive analysis of thousands of proteins

using a combination of SDS-PAGE and mass spectrometry without isotopic labeling.[21–23] For the transcriptomic analysis, we used publicly available transcriptomic data for GIST. We identified 18 genes whose expressions differed between S-GIST and I-GIST at both the protein and mRNA levels. Among the 18 genes, we found that promyelocytic leukemia (*PML*), a tumor suppressor gene, was significantly downregulated in I-GIST and S-GIST that showed postoperative recurrence. Finally, using immunohistochemistry, we validated the prognostic utility of PML in 254 additional cases of GIST from multiple clinical facilities.

Patients and Methods

Patients and clinical information. We examined tumor tissues from 164 GIST patients who underwent surgery at the National Cancer Center Hospital between July 1972 and December 2005. Fresh frozen tumor tissues from 8 GIST patients were used for proteomic analysis. The mutational status of the *KIT* and *PDGFRA* was determined as described previously,[24] and the clinicopathological data for the individual patients are summarized in Table 1. Formalin-fixed paraffin-embedded (FFPE) tissue sections from 156 other GIST cases were examined immunohistochemically for independent validation (Suppl. Table S1). We also immunohistochemically examined 98 GIST cases that underwent surgery at Niigata University Hospital between October 1982 and December 2005 (Suppl. Table S2). All patients underwent resection with curative intent, and did not receive either neoadjuvant or adjuvant therapy with imatinib. Diagnosis was based on the World Health Organization Classification of Tumors of the Digestive System,[25] including tumor size, mitotic rate, presence of epithelioid morphology, and expression of CD34 and KIT. Recurrence risk was classified according to the NIH consensus criteria based on tumor size and mitotic count.[26] This project was approved by the institutional review boards of the National Cancer Center and Niigata University.

Label-free proteomic analysis. Proteins were extracted from fresh frozen tissues as described previously.[24] Sixty microgram protein samples were separated by 12.5% SDS-PAGE. Each gel lane was cut into 24 pieces of equal size using a GridCutter (Gel Company, San Francisco, CA, USA), and each gel piece was subjected to in-gel tryptic digestion as described previously.[27] The final trypsin digests were subjected to liquid chromatography coupled with LTQ-Orbitrap XL mass spectrometer (Thermo Fisher Scientific, San Jose, CA, USA) (Fig. 1a). Peptide identification and protein quantification were performed using Mascot (version 2.2; Matrix Science, London, UK) and Progenesis LC-MS version 3.4 (Nonlinear Dynamics, Newcastle, UK), respectively. Details of the mass spectrometric analysis are provided in the supporting information (Suppl. Doc. S1). The processed raw data for protein abundance was loaded to Expressionist analyst (GeneData, Basel, Switzerland), and subjected to quantile normalization, hierarchical clustering analysis, principal component analysis and statistical analysis using Welch's *t*-test.

Transcriptomic analysis. A publicly available microarray dataset (GSE8167), which had been previously generated using GeneChip Human Genome U133 Plus 2.0 arrays (Affymetrix, Santa Clara, CA, USA),[20] was obtained from the NCBI GEO database. The clinicopathological data for the 32 analyzed samples are summarized in Supplementary Table S3. Downloaded CELL files were imported into GeneSpring GX version 11.0 (Agilent Technologies, Santa Clara, CA, USA), and background correction, probe summarization and normalization were performed according to the RMA algorithm.[28] From the total of 54 675 probes, we extracted 6146 corresponding to the genes that had been observed in proteomic analysis. These probes were filtered according to the percentile of their signal intensities in the raw data (20-100th percentile). Among the remaining 6004 probes, hierarchical clustering analysis, principal component analysis, and statistical analysis using unpaired *t*-test with Benjamini and Hochberg's correction were performed (Fig. 1a).

Western blotting. Five microgram protein samples extracted from fresh frozen tumor tissues were separated by 12.5% SDS-PAGE and subsequently transferred to PVDF membranes. The separated proteins were reacted with a primary antibody against PML (1:500; Abcam, Cambridge, UK) at room temperature for 1 h, followed by a secondary antibody against rabbit IgG (1:2000; GE Healthcare Biosciences, Uppsala, Sweden) under the same conditions. The immune complex was detected by ECL Prime (GE Healthcare Biosciences) and LAS-3000 (Fuji Photo Film, Tokyo, Japan). The intensity of PML bands was normalized by that of the corresponding total lanes stained with Ponceau S using ImageQuant (GE Healthcare Biosceiences).

Immunohistochemistry. Promyelocytic leukemia expression was examined immunohistochemically using FFPE tissues, as described in our previous report.[24] In brief, 4-μm-thick tissue sections were autoclaved in 10 mmol/L citrate buffer (pH 6.0) at 121°C for 30 min and incubated with the antibody against PML (1:500; Abcam) at room temperature for 1 h. Immunostaining was carried out by the streptavidin–biotin peroxidase method using the Strept ABC Complex/HRP kit (Dako, Glostrup, Denmark). One pathologist (A.Y.) and one clinician (H.I.), both blinded to the clinical data, reviewed the sections stained with anti-PML antibody. Tumor cells were

Table 1. Clinicopathological characteristics of the samples used in the proteomic analysis

Sample number	Anatomical tumor site	Gene mutation type	Histologic subtypes	Size (cm)	Mitosis (/50 HPF)	Risk classification†	Recurrence
1	Stomach	Wild type of *KIT* and *PDGFRA*	Spindle	3.5	≤5	Low	Absence
2	Stomach	Wild type of *KIT* and *PDGFRA*	Spindle	4.0	≤5	Low	Absence
3	Stomach	*KIT* exon 11 deletion	Mixed	12.0	>10	High	Peritoneum
4	Stomach	*KIT* exon 11 deletion	Mixed	4.0	>10	High	Liver
5	Small intestine	*KIT* exon 9 insertion	Spindle	3.7	≤5	Low	Absence
6	Small intestine	*KIT* exon 11 deletion	Spindle	7.0	≤5	Intermediate	Absence
7	Small intestine	*KIT* exon 11 deletion	Spindle	18.0	6–10	High	Liver
8	Small intestine	*KIT* exon 9 deletion	Mixed	7.0	>10	High	Peritoneum

†Recurrence risk was classified according to NIH consensus criteria. HPF, high power field of the microscope.

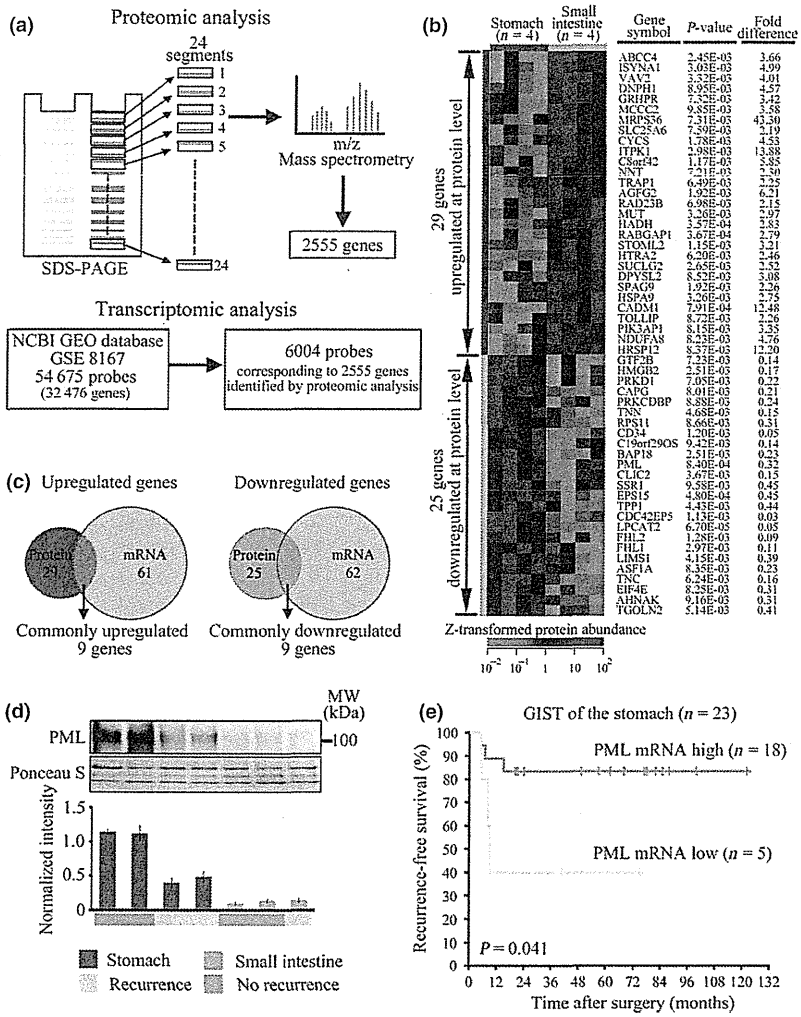

Fig. 1. Integrated proteomic and transcriptomic analysis shows promyelocytic leukemia (PML) downregulation in gastrointestinal stromal tumors (GIST) of the small intestine (I-GIST), and its potential as a prognostic biomarker. Workflow of the proteomic and transcriptomic analysis (a). Heatmap of the genes differentially expressed at the protein level (b). Venn diagrams showing the numbers of commonly upregulated and downregulated genes at both the protein and mRNA levels (c). Western blotting shows the differences in PML expression between the samples used for proteomic analysis (d). Kaplan–Meier analysis of recurrence-free survival according to the expression of PML mRNA in S-GIST of GSE8167 (e).

defined as positively stained if their nuclear staining intensity with the anti-PML antibody was equal to or higher than that of vascular endothelial cells used as an internal positive control in the same section. The examined cases were divided into negative (positive nuclear staining in <10% of tumor cells), focally positive (in ≥10% or more but <50%) and diffusely positive (in ≥50%), as previously reported.[29] In most cases, the difference was quite obvious and the two reviewers concurred as to the results.

Statistical analysis. Fisher's exact test was used to evaluate the correlations between PML expression status and clinicopathological characteristics. The correlation coefficients between these variables were evaluated using Spearman rank correlation analysis. The RFS was calculated from the date of initial surgery to that of first recurrence, censoring patients alive at the time of data collection and those who died without recurrence on the date of death. The RFS rate was estimated using the Kaplan–Meier method.[30] Univariate survival analyses were performed using the log-rank test. The Cox proportional hazards model was applied to the multivariate survival analysis.[31] The variables with a univariate $P < 0.05$ were entered into the model. Differences at $P < 0.05$ were regarded as statistically significant. SPSS version 11.5 (SPSS, Chicago, IL, USA) was used for all of the statistical analyses.

Results

Genes showing differences in protein expression specific to the tumor site. Using label-free proteomic analysis, we identified and quantified 26 832 unique peptides corresponding to 2550 non-redundant proteins from 8 GIST (Suppl. Tables S4 and S5). Unsupervised analysis showed that the samples were grouped according to the tumor site and whether or not the tumor recurred (Suppl. Fig. S1). These observations suggested that the overall protein expression profiles reflected the difference in the tumor site and malignant potential. Among the 2550 genes, 29 were significantly upregulated and 25 were

Table 2. Upregulated or downregulated genes in GIST of the small intestine at both protein and mRNA level

Gene symbol†	Gene description	Locus	Protein			mRNA			
			Accession number‡	*P*-value§	Fold difference¶	Probe set ID††	Accession number‡‡	*P*-value§§	Fold difference§
Upregulated genes									
ABCC4	Multidrug resistance-associated protein 4	13q32	O15439	2.45E-03	3.66	203196_at	AI948503	1.98E-03	3.27
						1554918_a_at	BC041560	6.27E-03	2.95
						1555039_a_at	AY133679	1.53E-03	2.69
AGFG2	Arf-GAP domain and FG repeats-containing protein 2	7q22.1	O95081	1.92E-03	6.21	206821_x_at	NM_006076	2.29E-04	2.87
						217450_at	AF053356	2.53E-05	2.91
						222126_at	AI247494	8.07E-04	5.04
						222362_at	H07885	6.96E-04	4.28
						1554618_at	BC009393	4.35E-04	3.20
ISYNA1	Inositol-3-phosphate synthase 1		O43598	8.95E-03	4.57	222240_s_at	AL137749	8.27E-03	2.11
CYCS	Cytochrome c	7p15.3	P99999	1.78E-03	4.53	208905_at	BC005299	2.46E-05	2.22
						229415_at	BF593856	5.12E-04	2.44
						244546_at	AI760495	8.34E-04	2.22
ITPK1	Inositol-tetrakisphosphate 1-kinase	14q31	Q13572	2.98E-03	13.88	210197_at	BC003622	4.91E-04	2.22
						210740_s_at	AF279372	1.59E-08	15.38
CADM1	Cell adhesion molecule 1	11q23.2	Q9BY67	7.91E-04	12.48	209030_s_at	NM_014333	1.24E-05	20.96
						209031_at	AL519710	2.95E-05	25.62
						209032_s_at	AF132811	1.70E-06	9.96
						244345_at	AI627453	2.90E-05	2.17
DNPH1	2′-deoxynucleoside 5′-phosphate N-hydrolase 1	6p21.1	O43598	8.95E-03	4.57	204238_s_at	NM_006443	1.93E-03	2.69
						39817_s_at	AF040105	2.14E-04	2.06
C8orf42	Chromosome 8 open reading frame 42	8p23.3	Q86YL5	1.17E-03	5.85	226778_at	AI632224	7.35E-04	2.75
						230903_s_at	H11634	2.22E-05	3.40
PIK3AP1	Phosphoinositide 3-kinase adapter protein 1	10q24.1	Q6ZUJ8	8.15E-03	3.35	226459_at	AW575754	3.15E-05	6.55
						1554508_at	BC029917	5.64E-07	4.51
Downregulated genes									
AHNAK	Neuroblast differentiation-associated protein AHNAK	11q12.2	Q09666	9.16E-03	0.31	211986_at	BG287862	6.36E-03	0.45
PML	Promyelocytic leukemia	15q22	P29590	8.40E-04	0.32	235508_at	AW291023	1.88E-06	0.42
CLIC2	Chloride intracellular channel protein 2	Xq28	O15247	3.67E-03	0.15	213415_at	AI768628	1.02E-06	0.18
CD34	CD34 molecule	1q32	P28906	1.20E-03	0.05	209543_s_at	M81104	8.83E-08	0.07
LPCAT2	Lysophosphatidylcholine acyltransferase 2	16q12.2	Q7L5N7	6.70E-05	0.05	227889_at	AI765437	1.30E-06	0.06
						222833_at	AU154202	1.01E-05	0.24
						239598_s_at	AA789296	7.19E-03	0.34
FHL2	Four and a half LIM domains protein 2	2q12.2	Q14192	1.28E-03	0.09	202949_s_at	NM_001450	1.36E-06	0.15
EPS15	Epidermal growth factor receptor substrate 15	1p32	P42566	4.80E-04	0.45	217887_s_at	NM_001981	3.48E-07	0.45
						217886_at	BF213575	2.90E-07	0.47
PRKCDBP	Protein kinase C delta-binding protein	11p15.4	Q969G5	8.88E-03	0.24	213010_at	AI088622	1.41E-06	0.16
CDC42EP5	Cdc42 effector protein 5	19q13.42	Q6NZY7	1.13E-03	0.03	227850_x_at	AW084544	7.84E-08	0.16

†Gene symbols were derived from UniGene. ‡Accession numbers of proteins were derived from Swiss-Prot and NCBI nonredundant databases. §*P*-values were calculated by *t*-test. ¶Fold differences were calculated by dividing the mean normalized expression value of GIST of the small intestine samples by that of GIST of the stomach samples. ††Affymetrix Human Genome U133 Plus 2.0 Array probe set ID. ‡‡Accession numbers of genes were derived from GenBank database. §§*P*-values were calculated by *t*-test and corrected by Benjamini–Hochberg false discovery rate. GIST, gastrointestinal stromal tumors.

downregulated at the protein level in I-GIST ($P < 0.01$; fold difference ≥2.0, Fig. 1b and Suppl. Table S6).

Genes showing differences in mRNA expression specific to the tumor site. From the GSE8167 dataset, we extracted 6004 probes corresponding to the genes observed in the proteomic analysis (Suppl. Table S7). Similarly to the protein expression profiles, unsupervised analysis showed that the overall features of mRNA expression reflected the difference in the tumor site (Suppl. Fig. S2). Among the 2555 genes corresponding to the 6004 probes, 65 genes (115 probes) were significantly upregulated and 67 genes (108 probes) were downregulated at the mRNA level in I-GIST ($P < 0.01$; fold difference ≥2.0, Suppl. Fig. S3 and Suppl. Table S8).

Integrated proteomic and transcriptomic analysis. We observed the 54 and 132 genes that were differentially expressed at the protein and mRNA levels. A total of 9 genes

were commonly upregulated and 9 were commonly downregulated in I-GIST at both the protein and mRNA level (Suppl. Fig. 1c and Table 2). CD34 protein and mRNA had been previously reported to be downregulated in I-GIST,[10,15] and our present study identified CD34 as a commonly downregulated gene in I-GIST (Table 2). Therefore, the other genes that were identified in our study may also be potentially related to the tumor site, and probably contribute to the malignant behavior of I-GIST.

The promyelocytic leukemia gene (*PML*) was included among the 9 genes that were commonly downregulated (Table 2 and Fig. S4). PML protein was originally identified as a fusion partner of the retinoic acid receptor-α (RARα) in the transforming protein (PML-RARα) found in acute promyelocytic leukemias.[32] PML functions as a tumor suppressor that controls apoptosis, protein synthesis, the cell cycle, cellular proliferation and genomic stability.[33] Loss of PML has been reported in breast cancer, gastric cancer and small cell lung cancer, but not in GIST.[34] In addition, *PML* is located on chromosome 15q, which is frequently lost in I-GIST,[17] suggesting that the decreased level of PML might reflect genomic alteration in I-GIST. With these notions, we further explored PML expression in GIST and its clinical utility.

Promyelocytic leukemia as a potential novel prognostic marker in gastrointestinal stromal tumors. Western blotting of the samples used for proteomic analysis revealed that PML protein was downregulated in I-GIST, being consistent with the result of the proteomic analysis. Moreover, we found that PML protein was also downregulated in the tumor of S-GIST obtained from patients who developed postoperative recurrence (Fig. 1d). We then analyzed the expression of PML mRNA in 23 cases of S-GIST using the transcriptome dataset. The appropriate cut-off value for the prediction of postoperative recurrence was set at −0.094 with a sensitivity of 88.2% and a specificity of 50.0% by the receiver operating characteristic curve (Suppl. Fig. S5). We divided 23 cases into two groups showing high (n = 18) and low (n = 5) expression by this value. Kaplan–Meier analysis demonstrated

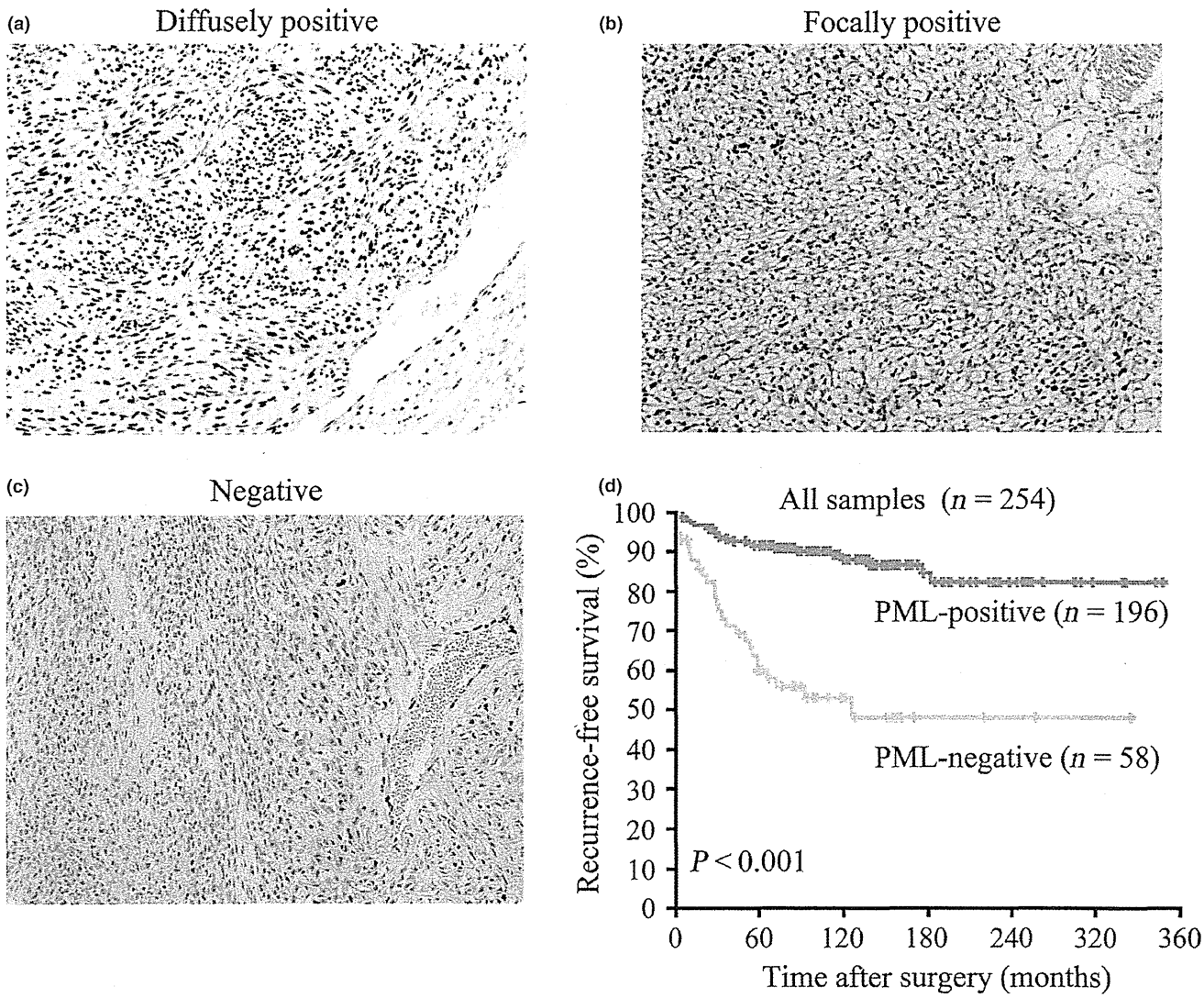

Fig. 2. Immunohistochemical validation study of promyelocytic leukemia (PML) expression. PML is diffusely positive in gastrointestinal stromal tumors (GIST) of the stomach (S-GIST) (a), whereas it is focally positive in S-GIST with recurrence (b), and it is not expressed in GIST of the small intestine (c). Kaplan–Meier analysis of recurrence-free survival according to PML expression in samples from multiple clinical facilities (d).

that the RFS period of patients with low expression of PML mRNA was significantly shorter than that of patients with high expression ($P = 0.041$) (Fig. 1e). PML was downregulated not only in I-GIST but also in S-GIST showing malignant behavior, and has the potential to be a novel prognostic marker in GIST.

Immunohistochemical validation study using gastrointestinal stromal tumor cases from multiple clinical facilities. We validated the correlation of PML expression with the tumor site and patients' outcome using immunohistochemistry in 254 additional samples from the National Cancer Center Hospital (156 cases) and Niigata University Hospital (98 cases). PML immunostaining showed a nuclear speckled pattern or a diffuse nucleoplasmic pattern (Fig. 2a–c). Vascular endothelial cells were strongly positive for PML expression, as described in a previous report.[34] Among the 254 cases, 196 cases (77.2%) showed diffusely positive staining and were classified as PML-positive. The remaining 46 cases (18.1%) showing focal positivity and 12 cases (4.7%) that were negative were classified as PML-negative. Thirty-six of 211 cases with S-GIST (17.0%), 12 of 22 cases with I-GIST (54.5%) and 10 of 21 cases arising in other organs (47.6%) showed PML-negative, the differences being statistically significant ($P < 0.001$). Expression of PML was also correlated with tumor size ($P < 0.001$), mitosis ($P < 0.001$) and NIH consensus criteria ($P < 0.001$) as well as the tumor site (Table 3). Kaplan–Meier survival analysis showed that the 5-year RFS rate was significantly lower for PML-negative than for PML-positive cases (60.1% *vs* 91.7%; $P < 0.001$) (Table 3 and Fig. 2d). Tumor site, histologic subtype, tumor size, mitosis and NIH consensus criteria were also significantly correlated with RFS in the univariate analysis. The correlation coefficient between NIH consensus criteria and tumor size was 0.78, and that between NIH consensus criteria and mitosis was 0.71 (Suppl. Table S9). They were especially high among those between other variables. Therefore, tumor size and mitosis were excluded from the variables entered into the Cox proportional hazards model to avoid multicollinearity. As a result, PML negativity was an independent unfavorable prognostic factor (hazard ratio [HR] = 2.739; $P = 0.001$) in addition to an indicator of a

Table 3. Correlations between clinicopathological characteristics and immunohistochemical expression of PML and survival analysis in the 254 GIST patients of the NCCH and Niigata University Hospital

Variable	Number of patients ($N = 254$)	PML expression		*P*-value	Univariate analysis		Multivariate analysis‡		
		Positive ($N = 196$)	Negative ($N = 58$)		5-year RFS rate (%)†	*P*-value	Hazard ratio	95% CI	*P*-value
Age									
<60	103	75	28	0.173	78.5	0.184	Not included		
≥60	151	121	30		88.8				
Gender									
Female	130	95	35	0.112	88.8	0.199	Not included		
Male	124	101	23		80.2				
Tumor site									
Stomach	211	175	36	<0.001	88.7	<0.001	1.000		
Small intestine	22	10	12		59.1		2.130	0.985–4.609	0.055
Other	21	11	10		71.1		1.531	0.686–3.418	0.298
Histologic subtype									
Spindle	198	157	41	0.350	90.7	<0.001	1.000		
Epithelioid	17	13	4		70.6		1.849	0.740–4.618	0.188
Mixed	37	25	12		57.0		1.699	0.859–3.359	0.128
Unknown§	2	1	1		—		—	—	—
Size (cm)									
≤5	154	132	22	<0.001	93.3	<0.001	Not included		
5.1–10.0	75	50	25		75.7				
>10	25	14	11		58.8				
Mitosis (/50 HPF)									
≤5	185	155	30	<0.001	95.0	<0.001	Not included		
6–10	43	27	16		73.2				
>10	26	14	12		28.2				
Risk classification¶									
Very low or low	122	107	15	<0.001	96.6	<0.001	1.000		
Intermediate	71	56	15		91.4		2.808	0.937–8.411	0.065
High	61	33	28		52.5		13.121	4.877–35.301	<0.001
PML expression									
Positive	196	—	—	—	91.7	<0.001	1.000		
Negative	58	—	—		60.1		2.739	1.498–5.006	0.001

†Five-year RFS rates were estimated by the Kaplan–Meier method. ‡In addition to PML expression status, covariates of tumor site, histologic subtype and recurrence risk classification were included in the multivariate analysis. §Two cases of unknown histologic subtype were not included in the survival analysis. ¶Recurrence risk was classified according to the NIH consensus criteria. CI, confidence interval; GIST, gastrointestinal stromal tumors; HPF, high power fields; PML, promyelocytic leukemia; RFS, recurrence-free survival.

high-risk of recurrence according to the NIH consensus criteria (HR = 13.121; $P < 0.001$).

We then examined the prognostic value of PML expression in cases stratified according to the tumor site or NIH consensus criteria (Fig. 3). In the S-GIST group, the 5-year RFS rate was 61.2% for PML-negative cases and 94.2% for PML-positive cases ($P < 0.001$; Fig. 3a). In contrast, in the I-GIST and other anatomical tumor site group, the difference between PML-positive and negative cases was not statistically significant (Fig. 3b,c). With regard to the NIH consensus criteria, the RFS rate was significantly lower in PML-negative than in PML-positive cases within each risk group (Fig. 3d–f).

Discussion

The prognosis of GIST patients differs according to the tumor site; I-GIST show more aggressive behavior than S-GIST.[11] Genome-wide global studies have revealed differences in *KIT* or *PDGFRA* mutations, gene expressions and chromosomal aberrations between I-GIST and S-GIST.[13–20] These observations suggest that further exploration of these molecular aberrations associated with the tumor site would yield clues to understanding the molecular background of the malignancy in GIST, thus widening the clinical options available to GIST patients.

This is the first report of the integrated proteomic and transcriptomic analysis of GIST aimed at exploring the molecular differences associated with the tumor site and prognostic biomarkers. The proteome is the functional translation of the genome, by which tumor cell phenotypes are directly regulated. Therefore, the proteomic analysis has considerable potential for discovery of biomarkers based on the molecular backgrounds of tumor malignancy. Proteomics can identify many proteins showing differential expressions. Thus, selection and validation of biomarker candidates is critical in the biomarker study. Recently, transcriptome data for well characterized clinical materials became publically available, and meta-analysis has been performed to assess the clinical utilities of biomarker candidates at the mRNA level. This is in contrast to proteome data, as few such data for clinical materials are publicly available. For proteins whose expression levels show concordance with those of the corresponding mRNA, it is possible to verify their utility as biomarkers using western blotting and immunohistochemistry at the protein level, or RT-PCR and meta-analysis of public transcriptomic data at the mRNA level. Against this background, we challenged the biomarker discovery at both the protein and mRNA levels.

We identified *PML* as a commonly downregulated gene in I-GIST at both the protein and mRNA levels. PML regulates oncogenic pathways such as the cell cycle, apoptosis and angiogenesis through interaction with pRB, p53, MDM2, PTEN, mTOR and HIF-1α.[33] *PML* is one of the tumor suppressor genes, and its loss leads to alteration of these pathways. These oncogenic pathways reported to play a major role in the molecular biology of GIST through the constitutive activation of KIT or PDGFRA signaling (Suppl. Fig. S6). GIST with high-risk of recurrence show significant changes in genes that regulate the cell cycle.[35] *TP53* mutations, p53 overexpression and *MDM2* amplification are correlated with poor outcome in GIST patients.[36,37] The PI3K-mTOR signaling pathway is one of the most important for growth of GIST cells.[38] HIF-1α plays an important role in GIST angiogenesis, and high expression is correlated with recurrence and metastasis.[39] Therefore, downregulation of PML might contribute to the malignant behavior of I-GIST.

We validated the association of PML expression with the tumor site and confirmed its prognostic utility in additional cases of GIST from multiple clinical facilities using immunohistochemistry. Downregulation of PML expression was significantly associated with not only I-GIST, but also a larger tumor size, higher mitotic count and higher risk of recurrence (Table 3). These results are consistent with the abovementioned tumor suppressive function of PML because these findings reflect higher cell proliferation based on dysregulation of the cell cycle or apoptosis. Survival analysis showed that PML expression was significantly correlated with the RFS period; identical results were obtained in cases stratified according to their institutions of origin (Suppl. Fig. S7 and S8; Suppl. Tables S10 and S11). The stratified survival analysis showed that PML expression was significantly correlated with the RFS period in the S-GIST group, but not in the I-GIST and other sites group. Therefore, PML could be applied as a prognosticator to patients with S-GIST. I-GIST and GIST arising from other sites were minorities in GIST, and the number of cases examined was small. Further analyses are needed to elucidate the benefit of PML evaluation in these types of GIST.

Recent studies indicated that adjuvant imatinib administration was relevant for NIH high-risk patients, but the evidence on intermediate-risk patients is insufficient.[9] In our analysis, prognostic significance of PML expression was independent from that of NIH consensus criteria. PML expression could clearly distinguish between better and worse prognosis of patients within the NIH intermediate-risk group, and the 5-year RFS rate of the PML-negative cases was 71.8%. Thus, PML evaluation to select patients suitable for adjuvant therapy with imatinib may be applicable to the intermediate-risk group. However, the difference of RFS according to PML expression in the NIH very low or low-risk group was statistically significant, but PML-negative cases had relatively good prognosis; the 5-year survival rate was 86.2%. Therefore, adjuvant imatinib administration is considered as over-treatment for patients in the NIH very low or low-risk group regardless of PML expression. However, further prospective analyses are necessary to clarify the utility of PML evaluation for an optimization of the adjuvant therapy.

Our study was limited in that we did not examine the molecular functions of PML *in vivo* and *in vitro*. Recently, inhibition of the PML degradation pathway using a proteasome inhibitor has been show to preserve its expression, thus making it an attractive approach for anti-cancer therapy.[40] We examined the effects of a proteasome inhibitor on PML protein expression in GIST cells (GIST-T1), and found that the inhibitor did not preserve PML protein expression, probably because it is controlled predominantly at the mRNA level and not at the protein degradation level in GIST cells (Suppl. Fig. S9). Further analysis of the functional significance of PML will lead to a more detailed understanding of the disease mechanisms of GIST, thus helping to reveal novel therapeutic modalities.

In conclusion, through integrated proteomic and transcriptomic analysis, we demonstrated differential expressions of 18 genes associated with the tumor site. Among them, we identified *PML*, a tumor suppressor gene, as a commonly downregulated gene at both the protein and mRNA levels in I-GIST. Using additional cases from multiple clinical facilities, we successfully validated the association of PML downregulation

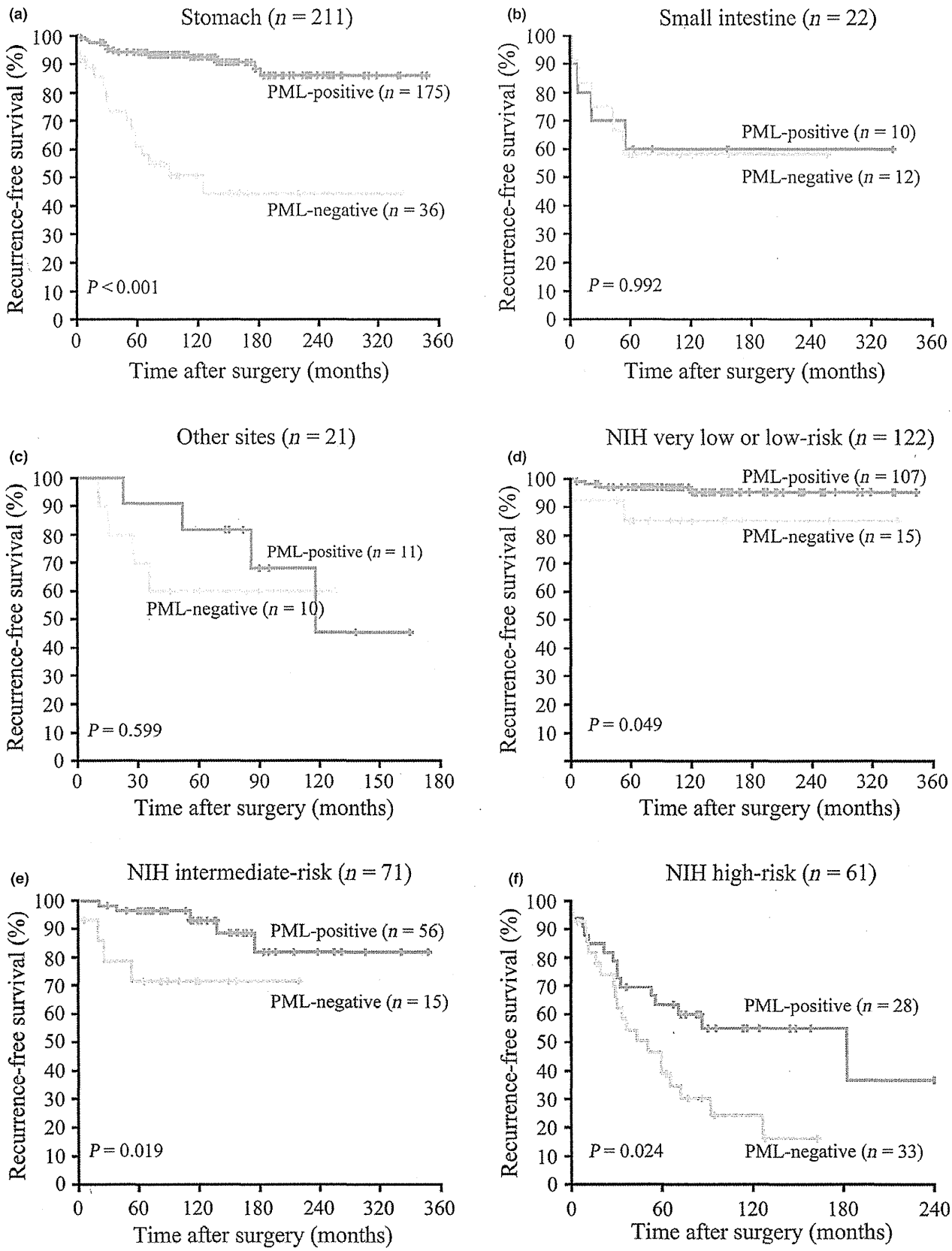

Fig. 3. The stratified Kaplan–Meier analysis of recurrence-free survival. The cases were stratified according to the tumor site (a–c), and stratified according to recurrence risk classification of the NIH consensus criteria (d–f).

with I-GIST and a shorter RFS period. Prognostication using PML expression may help to optimize the treatment strategy for GIST patients.

Disclosure Statement

The authors have no conflict of interest to declare.

References

1 Rubin BP, Heinrich MC, Corless CL. Gastrointestinal stromal tumour. *Lancet* 2007; **369**: 1731–41.
2 Hirota S, Isozaki K, Moriyama Y *et al.* Gain-of-function mutations of c-kit in human gastrointestinal stromal tumors. *Science* 1998; **279**: 577–80.
3 Hirota S, Ohashi A, Nishida T *et al.* Gain-of-function mutations of platelet-derived growth factor receptor alpha gene in gastrointestinal stromal tumors. *Gastroenterology* 2003; **125**: 660–7.
4 Heinrich MC, Corless CL, Duensing A *et al.* PDGFRA activating mutations in gastrointestinal stromal tumors. *Science* 2003; **299**: 708–10.
5 Corless CL, Barnett CM, Heinrich MC. Gastrointestinal stromal tumours: origin and molecular oncology. *Nat Rev Cancer* 2011; **11**: 865–78.
6 Dematteo RP, Ballman KV, Antonescu CR *et al.* Adjuvant imatinib mesylate after resection of localised, primary gastrointestinal stromal tumour: a randomised, double-blind, placebo-controlled trial. *Lancet* 2009; **373**: 1097–104.
7 Kanda T, Nishida T, Wada N *et al.* Adjuvant therapy with imatinib mesylate after resection of primary high-risk gastrointestinal stromal tumors in Japanese patients. *Int J Clin Oncol* 2013; **18**: 38–45.
8 Joensuu H, Eriksson M, Sundby Hall K *et al.* One vs three years of adjuvant imatinib for operable gastrointestinal stromal tumor: a randomized trial. *JAMA* 2012; **307**: 1265–72.
9 Joensuu H. Adjuvant treatment of GIST: patient selection and treatment strategies. *Nat Rev Clin Oncol* 2012; **9**: 351–8.
10 Miettinen M, Lasota J. Gastrointestinal stromal tumors – definition, clinical, histological, immunohistochemical, and molecular genetic features and differential diagnosis. *Virchows Arch* 2001; **438**: 1–12.
11 Emory TS, Sobin LH, Lukes L, Lee DH, O'Leary TJ. Prognosis of gastrointestinal smooth-muscle (stromal) tumors: dependence on anatomic site. *Am J Surg Pathol* 1999; **23**: 82–7.
12 Joensuu H. Risk stratification of patients diagnosed with gastrointestinal stromal tumor. *Hum Pathol* 2008; **39**: 1411–9.
13 Antonescu CR, Sommer G, Sarran L *et al.* Association of KIT exon 9 mutations with nongastric primary site and aggressive behavior: KIT mutation analysis and clinical correlates of 120 gastrointestinal stromal tumors. *Clin Cancer Res* 2003; **9**: 3329–37.
14 Haller F, Happel N, Schulten H-J *et al.* Site-dependent differential KIT and PDGFRA expression in gastric and intestinal gastrointestinal stromal tumors. *Mod Pathol* 2007; **20**: 1103–11.
15 Antonescu CR, Viale A, Sarran L *et al.* Gene expression in gastrointestinal stromal tumors is distinguished by KIT genotype and anatomic site. *Clin Cancer Res* 2004; **10**: 3282–90.
16 Chen Y, Tzeng C-C, Liou C-P, Chang M-Y, Li C-F, Lin C-N. Biological significance of chromosomal imbalance aberrations in gastrointestinal stromal tumors. *J Biomed Sci* 2004; **11**: 65–71.
17 Gunawan B, Schulten H-J, von Heydebreck A *et al.* Site-independent prognostic value of chromosome 9q loss in primary gastrointestinal stromal tumours. *J Pathol* 2004; **202**: 421–9.
18 Nishitani A, Hirota S, Nishida T *et al.* Differential expression of connexin 43 in gastrointestinal stromal tumours of gastric and small intestinal origin. *J Pathol* 2005; **206**: 377–82.
19 Wozniak A, Sciot R, Guillou L *et al.* Array CGH analysis in primary gastrointestinal stromal tumors: cytogenetic profile correlates with anatomic site and tumor aggressiveness, irrespective of mutational status. *Genes Chromosom Cancer* 2007; **46**: 261–76.
20 Yamaguchi U, Nakayama R, Honda K *et al.* Distinct gene expression-defined classes of gastrointestinal stromal tumor. *J Clin Oncol* 2008; **26**: 4100–8.
21 Schirle M, Heurtier M-A, Kuster B. Profiling core proteomes of human cell lines by one-dimensional PAGE and liquid chromatography-tandem mass spectrometry. *Mol Cell Proteomics* 2003; **2**: 1297–305.
22 Jafari M, Primo V, Smejkal GB, Moskovets EV, Kuo WP, Ivanov AR. Comparison of in-gel protein separation techniques commonly used for fractionation in mass spectrometry-based proteomic profiling. *Electrophoresis* 2012; **33**: 2516–26.
23 Li Z, Adams RM, Chourey K, Hurst GB, Hettich RL, Pan C. Systematic comparison of label-free, metabolic labeling, and isobaric chemical labeling for quantitative proteomics on LTQ Orbitrap Velos. *J Proteome Res* 2012; **11**: 1582–90.
24 Suehara Y, Kondo T, Seki K *et al.* Pfetin as a prognostic biomarker of gastrointestinal stromal tumors revealed by proteomics. *Clin Cancer Res* 2008; **14**: 1707–17.
25 Bosman FT, Carneiro F, Hruban RH, Theise ND. *WHO Classification of Tumours of the Digestive System*, 4th edn. Geneva: IARC Press, 2010.
26 Fletcher CD, Berman JJ, Corless C *et al.* Diagnosis of gastrointestinal stromal tumors: a consensus approach. *Hum Pathol* 2002; **33**: 459–65.
27 Kondo T, Hirohashi S. Application of highly sensitive fluorescent dyes (CyDye DIGE Fluor saturation dyes) to laser microdissection and two-dimensional difference gel electrophoresis (2D-DIGE) for cancer proteomics. *Nat Protoc* 2006; **1**: 2940–56.
28 Irizarry RA, Hobbs B, Collin F *et al.* Exploration, normalization, and summaries of high density oligonucleotide array probe level data. *Biostatistics* 2003; **4**: 249–64.
29 Lee HE, Jee CD, Kim MA *et al.* Loss of promyelocytic leukemia protein in human gastric cancers. *Cancer Lett* 2007; **247**: 103–9.
30 Kaplan EL, Meier P. Nonparametric estimation from incomplete observations. *J Am Stat Assoc* 1958; **53**: 457–81.
31 Cox D. Regression model and life tables. *J Royal Stat Soc* 1972; **B34**: 187–220.
32 Melnick A, Licht JD. Deconstructing a disease: RARalpha, its fusion partners, and their roles in the pathogenesis of acute promyelocytic leukemia. *Blood* 1999; **93**: 3167–215.
33 Salomoni P, Ferguson BJ, Wyllie AH, Rich T. New insights into the role of PML in tumour suppression. *Cell Res* 2008; **18**: 622–40.
34 Gurrieri C, Capodieci P, Bernardi R *et al.* Loss of the tumor suppressor PML in human cancers of multiple histologic origins. *J Natl Cancer Inst* 2004; **96**: 269–79.
35 Haller F, Gunawan B, von Heydebreck A *et al.* Prognostic role of E2F1 and members of the CDKN2A network in gastrointestinal stromal tumors. *Clin Cancer Res* 2005; **11**: 6589–97.
36 Zong L, Chen P, Jiang J, Wang L, Li QG. Predictive value of p53 expression in the risk of malignant gastrointestinal stromal tumors: evidence from 19 studies. *Exp Ther Med* 2012; **3**: 87–92.
37 Tornillo L, Duchini G, Carafa V *et al.* Patterns of gene amplification in gastrointestinal stromal tumors (GIST). *Lab Invest* 2005; **85**: 921–31.
38 Bauer S, Duensing A, Demetri GD, Fletcher JA. KIT oncogenic signaling mechanisms in imatinib-resistant gastrointestinal stromal tumor: PI3-kinase /AKT is a crucial survival pathway. *Oncogene* 2007; **26**: 7560–8.
39 Chen W-T, Huang C-J, Wu M-T, Yang S-F, Su Y-C, Chai C-Y. Hypoxia-inducible factor-1alpha is associated with risk of aggressive behavior and tumor angiogenesis in gastrointestinal stromal tumor. *Jpn J Clin Oncol* 2005; **35**: 207–13.
40 Chen R-H, Lee Y-R, Yuan W-C. The role of PML ubiquitination in human malignancies. *J Biomed Sci* 2012; **19**: 81.

Supporting Information

Additional supporting information may be found in the online version of this article:

Fig. S1. Unsupervised analysis according to the protein expression of 2555 genes.

Fig. S2. Unsupervised analysis according to the mRNA expression of 2555 genes.

Fig. S3. Heat-map of the 132 genes (223 probes) showing differences in mRNA expression between S-GIST and I-GIST.

Fig. S4. The difference in promyelocytic leukemia (PML) expression between S-GIST and I-GIST revealed by proteomic and transcriptomic analysis.

Fig. S5. Receiver operating characteristic curve of promyelocytic leukemia (PML) mRNA expression as a discriminator of recurrence status in the S-GIST group.

Fig. S6. Schema of the interaction between promyelocytic leukemia (PML) and gastrointestinal stromal tumors (GIST) oncogenic pathways lying downstream of KIT or PDGFRA.

Fig. S7. Immunohistochemical validation study of promyelocytic leukemia (PML) expression in the 156 gastrointestinal stromal tumors (GIST) cases from the National Cancer Center Hospital.

Fig. S8. Immunohistochemical validation study of promyelocytic leukemia (PML) expression in the 98 gastrointestinal stromal tumors (GIST) cases from Niigata University Hospital.

Fig. S9. Effects of a proteasome inhibitor, bortezonib, on promyelocytic leukemia (PML) expression in GIST-T1 cells.

Table S1. Clinicopathological characteristics of the 156 gastrointestinal stromal tumors (GIST) cases from the National Cancer Center Hospital.

Table S2. Clinicopathological characteristics of the 98 gastrointestinal stromal tumors (GIST) cases from Niigata University Hospital.

Table S3. Clinicopathological characteristics of the samples used in the transcriptomic analysis.

Table S4. Details of 2555 proteins analyzed by Progenesis LC-MS.

Table S5. Details of peptides assigned to 2555 proteins.

Table S6. Genes differentially expressed at the protein level in I-GIST.

Table S7. Details of 6004 probes corresponding to 2555 genes identified in the proteomic analysis.

Table S8. Genes differentially expressed at the mRNA level in I-GIST.

Table S9. The correlation coefficients between the clinicopathological characteristics.

Table S10. Correlations between clinicopathological characteristics and immunohistochemical expression of promyelocytic leukemia (PML) and survival analysis in gastrointestinal stromal tumors (GIST) cases from the National Cancer Center Hospital.

Table S11. Correlations between clinicopathological characteristics and immunohistochemical expression of promyelocytic leukemia (PML) and survival analysis in gastrointestinal stromal tumors (GIST) cases from Niigata University Hospital.

Doc. S1. Supporting materials and methods.

Journal of proteome research

Article

pubs.acs.org/jpr

Global PROTOMAP Profiling to Search for Biomarkers of Early-Recurrent Hepatocellular Carcinoma

Masato Taoka,[†] Noriaki Morofuji,[▽,‡] Yoshio Yamauchi,[†] Hidenori Ojima,[○,§] Daisuke Kubota,[‡] Goro Terukina,[†] Yuko Nobe,[†] Hiroshi Nakayama,[∥] Nobuhiro Takahashi,[⊥] Tomoo Kosuge,[#] Toshiaki Isobe,[*,†] and Tadashi Kondo[*,‡]

[†]Department of Chemistry, Graduate School of Sciences and Engineering, Tokyo Metropolitan University, Minamiosawa 1-1, Hachioji-shi, Tokyo 192-0397, Japan

[‡]Division of Pharmacoproteomics and [§]Division of Molecular Pathology, National Cancer Center Research Institute, 5-1-1 Tsukiji, Chuo-ku, Tokyo 104-0045, Japan

[∥]Biomolecular Characterization Team, RIKEN Advanced Science Institute, 2-1, Hirosawa, Wako, Saitama 351-0198, Japan

[⊥]Department of Biotechnology, United Graduate School of Agriculture, Tokyo University of Agriculture and Technology, Saiwai-cho 3-5-8, Fuchu-shi, Tokyo 183-8509, Japan

[#]Hepatobiliary and Pancreatic Surgery Division, National Cancer Center Hospital, 5-1-1 Tsukiji, Chuo-ku, Tokyo 104-0045, Japan

Supporting Information

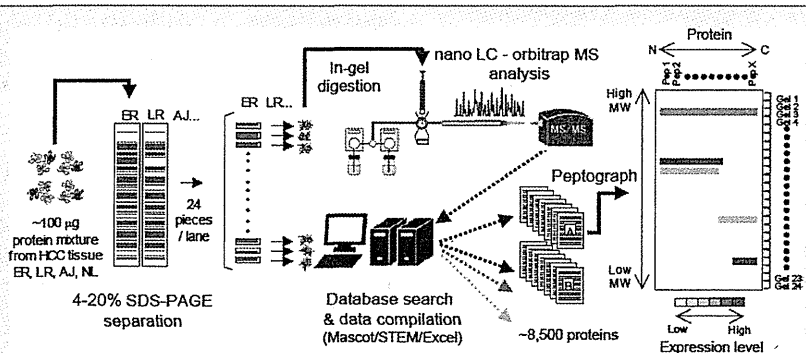

ABSTRACT: This study used global protein expression profiling to search for biomarkers to predict early recurrent hepatocellular carcinoma (HCC). HCC tissues surgically resected from patients with or without recurrence within 2 years (early recurrent) after surgery were compared with adjacent nontumor tissue and with normal liver tissue. We used the PROTOMAP strategy for comparative profiling, which integrates denaturing polyacrylamide gel electrophoresis migratory rates and high-resolution, semiquantitative mass-spectrometry-based identification of in-gel-digested tryptic peptides. PROTOMAP allows examination of global changes in the size, topography, and abundance of proteins in complex tissue samples. This approach identified 8438 unique proteins from 45 708 nonredundant peptides and generated a proteome-wide map of changes in expression and proteolytic events potentially induced by intrinsic apoptotic/necrotic pathways. In the early recurrent HCC tissue, 87 proteins were differentially expressed (≥20-fold) relative to the other tissues, 46 of which were up-regulated or specifically proteolyzed and 41 of which were down-regulated. This data set consisted of proteins that fell into various functional categories, including signal transduction and cell organization and, notably, the major catalytic pathways responsible for liver function, such as the urea cycle and detoxification metabolism. We found that aberrant proteolysis appeared to occur frequently during recurrence of HCC in several key signal transducers, including STAT1 and δ-catenin. Further investigation of these proteins will facilitate the development of novel clinical applications.

KEYWORDS: *hepatocellular carcinoma, biomarker, PROTOMAP, proteomics, mass spectrometry*

INTRODUCTION

Hepatocellular carcinoma (HCC) is one of the most common and aggressive malignancies and is the third leading cause of cancer deaths worldwide.[1] Although early diagnosis and subsequent treatments have considerably improved overall survival, long-term survival rates remain low because of a high

Special Issue: Proteomics of Human Diseases: Pathogenesis, Diagnosis, Prognosis, and Treatment

Received: March 14, 2014

dx.doi.org/10.1021/pr500262p | *J. Proteome Res.* XXXX, XXX, XXX−XXX

incidence of recurrence and metastasis.[2−7] Several pathological and clinical parameters are used to assess the malignant features of HCC and predict the prognosis after treatment, including histological differentiation, size of tumor, vascular invasion, and liver function.[8] However, a substantial subset of HCC tumors that are classified as low risk still progress to metastasis after treatment. Further investigation of the underlying mechanisms that determine malignant potential in HCC is necessary to optimize therapeutic strategies for individual patients.

Global gene and protein expression studies of primary tumor tissues have been a central tool in the development of prognostic biomarkers for HCC. Iizuka et al. examined mRNA expression in tissues of patients with different prognoses and identified a set of 12 genes associated with recurrence.[9] Ye et al. also identified a gene expression signature for the metastatic potential of HCC through global gene expression analysis.[10] These studies also provide insight into the malignant features of HCC.[11]

Using a 2-D difference gel-electrophoresis-based proteomics approach, we identified adenomatous polyposis coli (APC)-binding protein EB1 as a prognostic biomarker for HCC.[12] Similar studies identified calpain small subunit 1,[13] mortalin,[14] and talin-1[15] as prognostic biomarker candidates from clinical samples. Although these studies show the utility of proteomics in identifying biomarkers, posttranslational modifications of proteins were not considered in these studies.

Tissue homeostasis is severely disrupted in HCC by excessive proliferation of apoptosis-resistant cancer cells, which can alter the degree of caspase-related proteolysis.[16,17] This proteolysis is a key regulatory mechanism of normal physiological processes that promote development,[18,19] blood coagulation,[20] and cell death,[21] and proteolytic dysfunction is associated with many pathological events such as infectious disease[22] and cancer.[23] To date, ~100 specific proteolysis-related hereditary diseases have been recognized, and for many of these diseases the levels of aberrant proteolytic fragments correlate with the severity of symptoms.[24] In fact, several proteolytic fragments, such as the ectodomain fragment derived from epithelial growth factor receptor-2[25] and the soluble fragment from cytokeratin 19,[26] have been found in the biological fluids of cancer patients and are considered potential cancer biomarkers. Thus, analysis of proteolytic events may be particularly useful in searching for prognostic biomarkers for HCC.

Recently, a novel proteomics approach, referred to as the Protein Topography and Migration Analysis Platform (PROTOMAP), was established to examine proteolytic events.[27] In this method, a sample mixture is first separated by conventional sodium dodecyl sulfate-polyacrylamide gel electrophoresis (SDS-PAGE), the gel lanes are cut into bands at fixed intervals, the cut bands are digested with trypsin, and the released peptides are analyzed by reversed-phase liquid chromatography−tandem mass spectrometry (LC−MS/MS). The resulting proteomic data are integrated into peptographs, which plot sequence coverage for a given protein in the horizontal dimension versus SDS-PAGE migration in the vertical dimension; thus, proteins that undergo proteolytic cleavage are identified by shifts in migration from higher to lower molecular weight species. This method has been used to generate a proteome-wide map of proteolytic events induced by the intrinsic apoptotic pathway and has uncovered many previously undocumented caspase substrates.[27] Similarly, the PROTOMAP method has been used to examine differences in metastatic potential in liver cancer cell lines, and these studies revealed that calpain-2 and related proteins are associated with liver cancer metastasis.[28]

Here we applied the PROTOMAP strategy for global comparative profiling of HCC to identify novel biomarkers that could be used to evaluate malignancy and predict recurrence. We performed large-scale comparative proteomic profiling of HCC tissues surgically resected from patients with or without recurrence within 2 years after surgery-early recurrent (ER)- and late-recurrent (LR)-HCC tissues, respectively, as well as of adjacent nontumor tissue and normal liver tissue. To improve the accuracy of the quantitative index, we modified the original procedure by replacing simple spectral counts with the exponentially modified protein abundance index (emPAI).[29] Our analysis generated a large data set of HCC differentiation- and malignancy-associated proteins and proteolytic products that may serve as useful prognostic and therapeutic targets to prevent HCC recurrence.

MATERIALS AND METHODS

Chemicals and Antibodies

All chemicals used in this study were obtained from Wako Pure Chemical Industries (Osaka, Japan), unless otherwise indicated. Antibodies against the Signal Transducers and Activators of Transcription family protein 1 (STAT1) C-terminal sequences (#9175), δ-catenin (#610133), and actin (#A5060) were purchased from Cell Signaling Technology (Danvers, MA), BD Biosciences (San Jose, CA), and Sigma-Aldrich (St. Louis, MO), respectively.

Patients and Tissue Samples

All tissues used in this study were obtained from patients at the National Cancer Center Hospital, Tokyo, Japan. Clinical and pathological information for these patients is summarized in Supplementary Table 1 in the Supporting Information. The diagnosis of liver cancer was made by ultrasonography and dynamic computed tomography or magnetic resonance imaging, and the diagnosis of HCC was confirmed by pathological examination of the resected tissues after surgery. From the patients with HCC, tissues were obtained at a time of initial surgery. The HCC patients had recurrence within 2 years after the surgery (ER-HCC) or did not have recurrence within the same term (LR-HCC). The nontumor tissues adjacent to the tumor (AJ), all but two of which had developed hepatitis or cirrhosis, were also collected at the time of surgery. These tissues did not have micro metastasis, as examined by microscopic inspection. The normal liver tissues (NL) were obtained from liver of the colorectal cancer patients who had recurrence in liver. While all patients with early recurrence exhibited portal vein invasion, the patients in the LR-HCC group did not have it. All but two patients with early recurrence had recurrent tumor(s) in remnant liver (Supplemental Table 1 in the Supporting Information). Although we could not exclude the possibility that the early recurrence might include possible incomplete resection, we included all such cases in this study. The virus infection was observed in 16 cases of 20 HCC patients who provided tumor tissues in this study (Supplemental Table 1 in the Supporting Information). All tissues were immediately frozen at −80 °C after surgery. The Ethics Committee of National Cancer Center approved this study, and all patients participating in this study provided written, informed consent. We performed all experiments under the strict risk management to prevent virus infection according to the regulations of National Cancer Center Research Institute.

dx.doi.org/10.1021/pr500262p | J. Proteome Res. XXXX, XXX, XXX−XXX

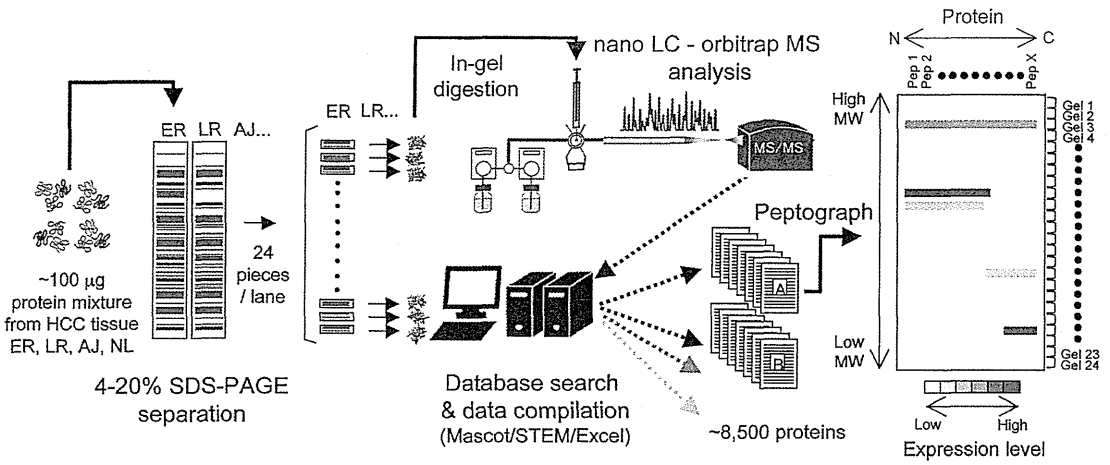

Figure 1. Schematic illustration of PROTOMAP strategy used in this study. Details are given in the text.

Sample Preparation, SDS-PAGE, LC–MS/MS Analysis, and Peptograph Assembly

The experimental procedure used in this study is illustrated in Figure 1. Tissue samples (100 μg protein) were separated by 4–20% SDS-PAGE, and the gel lanes were cut into 24 pieces at fixed intervals (0.5 cm bands). Each gel piece was incubated with 0.25 μg trypsin in 20 μL of Tris-HCl (pH 8.8) overnight at 37 °C,[30] and the resulting peptide mixture was analyzed on a direct nanoflow LC–MS/MS system equipped with an Orbi-Trap mass spectrometer (Orbi-Trap XL, Thermo Scientific, Boston, MA), as described.[31] In brief, peptides were separated on a reversed-phase tip column (150 μm [i.d.] × 70 mm, Mightysil-C18, 3 μm particle) using a linear gradient starting at 100% A [A: 0.1% (v/v) formic acid in water] at 100 nL/min. The mobile phase was 0–35% B [B: 0.1% (v/v) formic acid in acetonitrile] for 70 min. The column was subsequently washed with 70% B for 10 min and re-equilibrated with 100% A for the next analysis. Full MS scans were acquired with a resolution of 30 000 at a mass-to-charge ratio of 400. The 10 most intense ions were fragmented in a data-dependent mode by collision-induced dissociation with normalized collision energy of 35, activation q of 0.25, and activation time of 10 ms and one microscan. The fragments were then analyzed in ion trap MS using the following conditions: spray voltage, 2.0 kV; ion transfer tube temperature, 200 °C; ion selection threshold, 10 000 counts; maximum ion accumulation times, 500 ms for full scans; and dynamic exclusion duration, 60 s (10 ppm window; maximum number of excluded peaks, 500). The MS/MS data were converted to the mascot generic format with the Proteome Discoverer software (Thermo Scientific, ver. 1.1). The files were processed with the MASCOT algorithm (version 2.2.1., Matrix Science, London, United Kingdom) to assign peptides using the Swiss-Prot sequence database (release 2011; 20 236 sequences, human) under the search parameters as described.[31] Peptide identifications were based on the MASCOT definitions, except that we used stricter protein assignment criteria than the standard defaults.[32] In brief, we set the variable modification parameters for acetylation (protein N-terminus) and oxidation (Met). The maximum missed cleavage was set at 1 with a peptide mass tolerance of ±15 ppm. Peptide charges from +2 to +4 states and MS/MS tolerances of ±0.8 Da were allowed. We selected the candidate peptides with probability-based Mowse scores (total score) that exceeded their threshold, indicating a significant homology ($p < 0.05$), and referred to them as "hits". The criteria were based on the vendor's definitions (Matrix Science). Furthermore, we set more strict criteria for protein assignment: (1) any peptide candidate with an MS/MS signal number of <2 was eliminated from the "hit" candidates, regardless of the match score (total score minus threshold); (2) proteins with match scores exceeding 10 ($p < 0.005$) were referred to as "identified"; and (3) if the protein was identified with a single peptide candidate having a match score lower than 10, the original MS/MS spectrum was carefully inspected to confirm that the assignment was based on three or more y- or b-series ions. All results of peptide searches were extracted from the Mascot DAT files using the STEM[33] software, expressed as tab-delaminated text files, and pooled in a spreadsheet of Microsoft Excel (Excel 2010, Microsoft, Albuquerque, NM). The identified peptides were then grouped into each particular protein that the peptide can be produced and sorted according to its sequence using the commands defined by the vendor.

The resulting data were integrated into heat map "peptographs", as described by Dix et al.,[27] except that we used the emPAI parameters[29] instead of simple spectral counts to estimate semiquantitative differences in the identified peptides. Specifically, in the peptographs, identified peptides for a given protein were plotted in the vertical dimension (N to C terminus, top to bottom), and SDS-PAGE migration of the protein was plotted in the horizontal dimension (high to low molecular weight, left to right). The semiquantitative differences in proteins estimated by the emPAI are represented in the peptographs by the depth of blue color (light to dark, low to high abundance) using a spreadsheet program (Excel 2010).

To evaluate the levels of specific proteins in the ER-HCC, LR-HCC, AJ, and NL tissues, we estimated a sum of emPAI parameters (Σ_{emPAI}) from the corresponding peptographs. If the Σ_{emPAI} value for a given protein in the ER-HCC tissue was >20-fold higher than the values in the LR-HCC, AJ, and NL tissues, we tentatively designated the protein as up-regulated. Conversely, if the Σ_{emPAI} value for a protein in the ER-HCC tissue was >20-fold lower than the values in any other tissues, we tentatively designated the protein as down-regulated.

Western Blotting

Proteins (15 μg) in crude tissue extracts were separated by SDS-PAGE on 4–20% gradient gels (Criterion TGX, Bio-Rad,

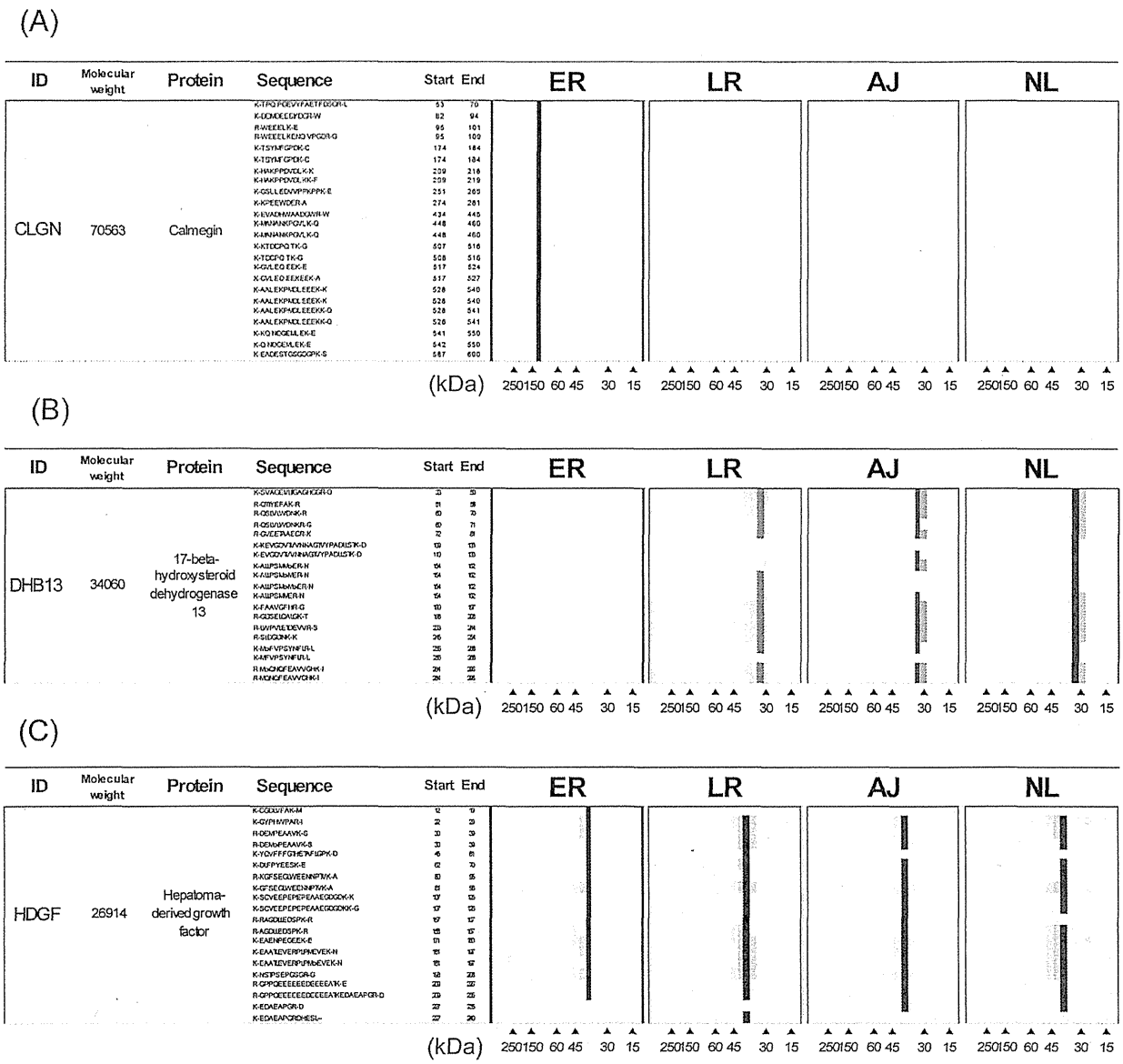

Figure 2. Representative peptographs of (A) calmegin, a protein that was up-regulated in ER-HCC tissue, (B) 17-β-hydroxysteroid dehydrogenase 13, a protein that was down-regulated in ER-HCC tissue, and (C) hepatoma-derived growth factor, a protein that did not appear to be affected by tumorigenesis. The vertical dimension shows the sequence of the identified protein from the N to the C terminus (top to bottom), and the horizontal dimension shows the SDS-PAGE–determined molecular weights (high to low, left to right, indicated at the bottom). The semiquantitative differences in protein and degradation product abundance, estimated by the emPAI, are reflected in the depth of the blue color (dark to light, high to low).

Hercules, CA) and transferred electrophoretically to polyvinylidene difluoride membranes (Trans-Blot Turbo, Bio-Rad). The membranes were blocked with StartingBlock blocking buffer (Thermo Scientific, Bremen, Germany) for 1 h at room temperature and then incubated with the appropriate antibodies overnight at 4 °C. The membranes were washed three times with StartingBlock blocking buffer for 10 min, incubated with horseradish peroxidase-conjugated secondary antibodies (1:10 000 dilution; GE Healthcare Bio-Sciences (Uppsala, Sweden) for 1 h at room temperature, washed three times with StartingBlock blocking buffer for 1 h, and visualized by enhanced chemiluminescence on Hyperfilm (GE Healthcare).

RESULTS AND DISCUSSION

Generation of Peptographs of HCC and Surrounding Liver Tissues

Proteins in crude extracts of the ER- and the LR-HCC tissues as well as the AJ and NL controls were separated in parallel lanes by SDS-PAGE. Samples 18 (NL), 24 (AJ), 37 (LR), and 16 (ER) were examined (Supplemental Table 1 in the Supporting Information). Immediately after electrophoresis, each sample lane was cut into 24 gel pieces at fixed intervals, and the proteins in each piece were in-gel digested with trypsin and analyzed by nanoflow reversed-phase LC–MS/MS for

dx.doi.org/10.1021/pr500262p | J. Proteome Res. XXXX, XXX, XXX–XXX

Table 1. Proteins Up-Regulated in the ER-HCC Tissue

UniProt ID	protein	molecular mass (kDa)	ΣemPAI maximum	degradation detected	oxido-reductase[a]	liver-specific expression[b]	phospho-protein[a]	previously reported HCC marker	ref
STAT1_HUMAN	signal transducer and activator of transcription 1-alpha/beta	87990	294.4	+	–	–	+	–	
GAGB1_HUMAN	G antigen family B member 1	16354	77.5	+	–	–	+	–	
CLGN_HUMAN	calmegin	70663	75.3	–	–	–	+	–	
LASP1_HUMAN	LIM and SH3 domain protein 1	30195	683	+	–	–	+	–	
SFPQ_HUMAN	splicing factor, proline- and glutamine-rich	76244	465	+	–	–	+	–	
PDIA2_HUMAN	protein disulfide-isomerase A2	58596	40.1	–	–	–	–	–	
CTND1_HUMAN	catenin delta-1	108814	39.9	+	–	–	+	–	
CKAP4_HUMAN	cytoskeleton-associated protein 4	66125	37.6	+	–	–	+	–	
ACOX3_HUMAN	peroxisomal acyl-coenzyme A oxidase 3	78503	36.2	+	+	–	+	–	
CLIP1_HUMAN	CAP-Gly domain-containing linker protein 1	163070	34.5	–	–	–	+	–	
ILEU_HUMAN	leukocyte elastase inhibitor	42857	34.4	+	–	–	+	–	
GALK1_HUMAN	galactokinase	42814	33.5	+	–	–	–	–	
FINC_HUMAN	fibronectin	266935	32.3	–	–	–	+	+	47–49
SYVC_HUMAN	valyl-tRNA synthetase	141950	31 3	+	–	–	+	–	
SYAC_HUMAN	alanyl-tRNA synthetase, cytoplasmic	107667	28.4	+	–	–	+	–	
PABP1_HUMAN	polyadenylate-binding protein 1	70910	28.3	+	–	–	+	–	
LGAT1_HUMAN	acyl-CoA: lysophosphatidylglycerol acyltransferase 1	43345	27.4	–	–	–	–	–	
ACACA_HUMAN	acetyl-CoA carboxylase 1	267516	26.0	+	–	–	+	–	
LPP1_HUMAN	lipid phosphate phosphohydrolase 1	32633	25.5	–	–	+	–	–	
HSPB1_HUMAN	heat shock protein beta-1	22840	25.5	+	–	±	+	+	50–52
SERPH_HUMAN	serpin H1	46553	24.7	+	–	–	–	–	
DHSA_HUMAN	succinate dehydrogenase flavoprotein subunit	73924	24.6	+	+	–	+	–	
AKA12_HUMAN	A-kinase anchor protein 12	192077	24.2	+	–	–	+	–	
DYHC1_HUMAN	cytoplasmic dynein 1 heavy chain 1	536482	24.0	+	–	–	+	–	
1C12_HUMAN	HLA class 1 histocompatibility antigen, Cw-12 alpha chain	41428	24.0	+	–	–	+	–	
SYWC_HUMAN	tryptophanyl-tRNA synthetase, cytoplasmic	53558	23.8	+	–	–	+	–	
TBB2A_HUMAN	tubulin beta-2A chain	50372	23.3	+	–	–	+	–	
1A01_HUMAN	HLA class I histocompatibility antigen, A-1 alpha chain	41175	23.1	+	–	–	+	–	
CLIP2_HUMAN	CAP-Gly domain-containing linker protein 2	116335	23.0	+	–	–	+	–	
UBA7_HUMAN	ubiquitin-like modifier-activating enzyme 7	112832	22.7	+	–	±	–	–	
1A36_HUMAN	HLA class I histocompatibility antigen, A-36 alpha chain	41263	22.5	+	–	–	+	–	
TIF1B_HUMAN	transcription intermediary factor 1-beta	90696	22.2	+	–	±	+	–	
TCPB_HUMAN	T-complex protein 1 subunit beta	57878	22.0	+	–	–	–	+	53
HNRPK_HUMAN	heterogeneous nuclear ribonucleoprotein K	51300	21 7	+	–	–	+	–	
HIP1R_HUMAN	huntingtin-interacting protein 1 -related protein	120167	21 6	–	–	+	+	–	
1C14_HUMAN	HLA class 1 histocompatibility antigen, Cw-14 alpha chain	41380	21.5	+	–	–	+	–	
AP3B1_HUMAN	AP-3 complex subunit beta-1	121955	21.3	+	–	±	+	–	
CO2_HUMAN	complement C2	84919	21.1	–	–	–	–	–	
1C04_HUMAN	HLA class I histocompatibility antigen, Cw-4 alpha chain	41467	21.0	+	–	–	+	–	
VIGLN_HUMAN	vigilin	142150	20.9	+	–	–	+	–	
ADRO_HUMAN	NADPH:adrenodoxin oxidoreductase, mitochondrial	54371	20.9	+	+	–	–	–	

dx.doi.org/10.1021/pr500262p | J. Proteome Res. XXXX, XXX, XXX–XXX

Table 1. continued

UniProt ID	protein	molecular mass (kDa)	ΣemPAI maximum	degradation detected	oxido-reductase[a]	liver-specific expression[b]	phospho-protein[a]	previously reported HCC marker	ref
DX39B_HUMAN	spliceosome RNA helicase DDX39B	49528	20.6	+	–	–	–	–	
FKBP4_HUMAN	peptidyl-prolyl cis–trans isomerase FKBP4	52127	20.4	+	–	±	+	–	
ACSL4_HUMAN	long-chain-fatty-acid-CoA ligase 4	80486	20.3	+	–	–	–	+	54
SYQ_HUMAN	glutaminyl-tRNA synthetase	88879	20.2	+	–	–	+	–	
HYOU1_HUMAN	hypoxia up-regulated protein 1	111550	20.1	+	–	++	–	–	

[a]According to the UniProt database. [b]±, ubiquitous; +, moderately specific; ++, highly specific.

protein identification. Duplicate analysis of each sample set identified 6218, 5857, 6010, and 5495 unique proteins based on 31 747, 31 419, 29 471, and 25 982 nonredundant peptides in the ER-HCC, LR-HCC, AJ, and NL tissues, respectively (Supplementary Table 2–5 in the Supporting Information). Overall, 8438 unique proteins were identified in the HCC and surrounding liver tissues (Supplementary Table 6 in the Supporting Information), which fell into a wide range of molecular weights (ranging from 5 kDa for thymosin β-10 to 3850 kDa for titin), subcellular compartments, and biological processes (Supplementary Figure 1A–C in the Supporting Information). The data sets obtained from the tissue samples were then integrated into peptographs (Supplementary Table 6 in the Supporting Information), which display differences in protein profiles between tissues on a proteome-wide scale. The peptographs also allowed visualization of potential proteolytic events that might be induced by the intrinsic apoptotic or necrotic proteolytic pathways during tumorigenesis. Representative portions of some of the peptographs are shown in Figure 2A–C.

Proteins Characteristic of ER-HCC Tissue

To search for ER-HCC–specific marker candidates, we focused on the proteins or proteolytic fragments that were specifically up- or down-regulated in the ER-HCC tissue. We selected 46 proteins that were up-regulated in ER-HCC tissue and 41 that were down-regulated (Tables 1 and 2). According to DAVID (Database for Annotation, Visualization and Integrated Discovery; http://david.niaid.nih.gov) categorization, the up-regulated proteins were involved in various cellular processes, including signal transduction, tRNA aminoacylation, protease inhibition, protein folding, and cell organization. Interestingly, we found that most of these up-regulated proteins (38/46) were specifically proteolyzed in the ER-HCC tissue (Table 1), and, according to the DAVID analysis, many of those (30/38) are potential phosphoproteins. Although the biological significance of this finding is unclear, it may be that atypical phosphoprotein degradation occurs in ER-HCC tissues, which inhibits normal phosphorylation-mediated signal transduction. As discussed in greater detail later, the peptograph analysis clearly detected proteolysis of two key phosphorylation-induced apoptotic signal transducers, STAT1 and δ-catenin, only in the ER-HCC tissue (Figure 3A,B).

We also found that several functional categories were overrepresented in the 41 down-regulated proteins detected in the ER-HCC tissue. First, 16 of the 41 proteins were oxidoreductases, consistent with previous reports that oxidoreductases are repressed in human, animal, and cultured hepatomas[34–39] (Table 2). For instance, levels of alcohol dehydrogenase 4 (ADH4) in HCC tissue are closely and negatively correlated with the pathology grade of the tumor and with levels of the tumor marker serum α-fetoprotein.[40] Likewise, HCC patients with low ADH4 expression levels have much lower overall survival rates than do those with high expression levels. In this study, we found that ADH4 levels were reduced in ER-HCC tissues and that the levels were substantially and negatively correlated with recurrence in patients with HCC. It should also be noted that 10 of the ER-HCC-specific proteins that we identified are previously known tumor marker candidates (Tables 1 and 2).

The down-regulated protein subset also contained many proteins that are liver-specific or are highly expressed in the liver and are involved in the catalytic pathways responsible for major liver functions, such as the urea cycle and detoxification metabolism. Of the 22 down-regulated proteins with available tissue distribution information in the UniProt database, 16 were categorized as specifically expressed or highly expressed in the liver, whereas only 3 of the 17 up-regulated proteins with tissue distribution information were categorized as liver-specific, suggesting that ER-HCC tissue contains many undifferentiated or dedifferentiated cells. Stem-like cells with their progeny have been observed in tumor tissues, and these cells have aberrant differentiation capacity or promote metastatic spread of tumor cells.[18,41] Taken together with our results, this suggests that stem-like cells that remain after surgery might cause early recurrence of HCC.

The results previously described indicate that the PROTOMAP strategy will be useful in the discovery of proteins associated with the malignant potential of HCC cells. Early recurrence of HCC was accompanied by portal vein invasion (Supplemental Table 1 in the Supporting Information), suggesting that aberrant regulation of the identified proteins may increase the invasiveness of tumor cells. Thus, these proteins are potential biomarkers for early recurrence and potential therapeutic targets.

Proteolytic Fragments of STAT1 and δ-Catenin

Our peptograph analysis detected proteolytic fragments of many proteins in HCC and surrounding liver tissues, particularly in ER-HCC tissue (Table 1). Although it is possible that some of these fragments were generated during storage or handling of tissue samples, this proteolysis might suggest that intrinsic apoptotic or necrotic proteolytic events contribute to tumorigenesis or recurrence of HCC. Of particular interest, we found that STAT1, a key transcriptional regulator in the Janus kinase (JAK)-STAT apoptotic pathway,[42] was much more abundant in ER-HCC tissue than in LR-HCC and surrounding liver tissues ($\Sigma_{emPAI} \approx 300$), and it was proteolyzed specifically in ER-HCC tissue (Figures 3A and 4A and Supplementary Table 6 in the Supporting Information).

Table 2. Proteins Down-Regulated in the ER-HCC Tissue

UniProt ID	protein	molecular mass (kDa)	ΣemPAI minimum	degradation detected	oxido-reductase[a]	liver-specific expression[a,b]	phospho-protein[a]	previously reported HCC marker	ref
CPSM_HUMAN	carbamoyl-phosphate synthase	166256	0.0033	−	−	++	+	+	55−57
HPPD_HUPMN	4-hydroxyphenylpyruvate dioxygenase	45119	0.0048	−	+	−	+	−	
HBB_HUMAN	hemoglobin subunit beta	16130	0.0057	−	−	−	−	−	
DHB13_HUMAN	17-beta-hydroxysteroid dehydrogenase 13	34060	0.0087	−	+	++	−	−	
SARDH_HUMAN	sarcosine dehydrogenase, mitochondrial	102180	0.0088	−	+	−	−	−	
HBA_HUMAN	hemoglobin subunit alpha	15319	0.0099	−	−	−	−	+	58
APOB_HUMAN	apolipoprotein B-100	516988	0.0101	−	−	−	−	−	
ADO_HUMAN	aldehyde oxidase	150805	0.0115	+	+	++	−	+	59
PALM3_HUMAN	paralemmin-3	72078	0.0134	+	−	−	+	−	
GPDA_HUMAN	glycerol-3-phosphate dehydrogenase	38326	0.0142	−	+	−	−	−	
F16P1_HUMAN	fructose-1,6-bisphosphatase 1	37316	0.0176	−	−	−	−	+	60,61
AK1D1_HUMAN	3-oxo-5-beta-steroid 4-dehydrogenase	37779	0.0211	−	+	++	−	−	
CP3A4_HUMAN	cytochrome P450 3A4	57803	0.0219	−	+	++	−	−	
APOA_HUMAN	apolipoprotein(a)	518115	0.0224	+	−	−	−	−	
HUTU_HUMAN	urocanate hydratase	75777	0.0227	−	−	−	−	−	
ADH4_HUMAN	alcohol dehydrogenase 4	41332	0.0239	−	+	−	−	+	40
MY18A_HUMAN	myosin-XVIIIa	234463	0.0242	+	−	−	−	−	
UD14_HUMAN	UDP-glucuronosyltransferase 1−4	60767	0.0245	+	−	++	−	−	
REEP6_HUMAN	receptor expression-enhancing protein 6	20933	0.0253	−	−	−	−	−	
DOPD_HUMAN	D-dopachrome decarboxylase	12846	0.0255	−	−	−	−	−	
GYS2_HUMAN	glycogen [starch] synthase, liver	81719	0.0264	−	−	−	+	−	
UD16_HUMAN	UDP-glucuronosyltransferase 1−6	61493	0.0271	−	−	++	−	−	
ARK73_HUMAN	aflatoxin B1 aldehyde reductase member 3	37680	0.0278	−	+	+	−	−	
GUAD_HUMAN	guanine deaminase	51610	0.0289	−	−	−	−	−	
DHTK1_HUMAN	probable 2-oxoglutarate dehydrogenase E1 component DHKTD	103935	0.0317	−	+	−	−	−	
UD13_HUMAN	UDP-glucuronosyltransferase 1−3	61009	0.0345	+	−	−	−	−	
MTP_HUMAN	microsomal triglyceride transfer protein large subunit	100070	0.0352	+	−	++	−	−	
UD19_HUMAN	UDP-glucuronosyltransferase 1−9	60967	0.0359	+	−	++	−	−	
MYLK_HUMAN	myosin light chain kinase	213993	0.0365	+	−	±	+	−	
FMO5_HUMAN	dimethylanilme monooxygenase 5	60750	0.0371	+	+	++	−	−	
UD18_HUMAN	UDP-glucuronosyltransferase 1−8	60626	0.0375	+	−	−	−	−	
UD15_HUMAN	UDP-glucuronosyltransferase 1−5	60742	0.0377	+	−	−	−	−	
ADH6_HUMAN	alcohol dehydrogenase 6	40271	0.0379	+	+	++	−	−	
HBD_HUMAN	hemoglobin subunit delta	16187	0.0381	−	−	−	−	−	
AASS_HUMAN	alpha-aminoadipic semialdehyde synthase	102990	0.0417	−	+	++	−	−	
AL1L1_HUMAN	aldehyde dehydrogenase family 1 member L1	99832	0.0427	−	+	++	−	+	62
DDTL_HUMAN	D-dopachrome decarboxylase-like protein	14470	0.0429	−	−	−	−	−	
CRYM_HUMAN	mu-crystallin homologue	33967	0.0439	−	−	−	−	−	
UD17_HUMAN	UDP-glucuronosyltransferase 1−7	60774	0.0451	+	−	++	−	−	
CP3A7_HUMAN	cytochrome P450 3A7	57915	0.0487	−	+	−	−	−	
HAOX1_HUMAN	hydroxyacid oxidase 1	41183	0.0500	−	+	++	−	−	

[a]According to the UniProt database. [b]±, ubiquitous; +, moderately specific; ++, highly specific.

The corresponding peptographs indicated that the full-length STAT1, with an apparent molecular mass of 90 kDa, appeared to be cleaved into two major fragments in ER-HCC, a 38-kDa N-terminal fragment and a 45-kDa C-terminal fragment, whereas these cleavage fragments were barely detectible in the LR-HCC, AJ, and NL tissues (Figures 3A and 4A). STAT1 contains several structurally and functionally conserved domains, including a coiled-coil STAT domain implicated in protein−protein interactions, a DNA-binding domain with an immunoglobulin-like fold, an SH2 domain that acts as a phosphorylation-dependent switch to control cytokine receptor recognition and DNA-binding, and a C-terminal transactivation domain.[43] Interestingly, our peptograph analysis showed that the specific proteolysis of STAT1 occurred within the linker region between the DNA binding and SH2 domains (residues 321−359). This implies that deregulation of the JAK-STAT pathway may play a role in HCC recurrence by inducing aberrant transcription of genes associated with cell proliferation or programmed cell death.

dx.doi.org/10.1021/pr500262p | J. Proteome Res. XXXX, XXX, XXX−XXX